

Numerical Analysis and Optimal CFD Model Verification of Piezoelectric Inkjet Printhead

T. Lei¹, J. Han^{1†} and H. Liu²

¹ School of Mechanical Engineering, Hefei University of Technology, Hefei, Anhui, China

² School of Mechatronic Engineering, North Minzu University, Yinchuan, Ningxia, China

†Corresponding Author Email: jianghan@hfut.edu.cn

(Received September 23, 2021; accepted March 17, 2022)

ABSTRACT

Flow dynamics accurate prediction is critical for the early-stage design and performance optimization of the piezoelectric (PZT) printhead. To achieve this, the Computational Fluid Dynamics (CFD) method has been widely used. However, for accurate fluid simulation of the PZT printhead, the optimal parameters settings still need to be clarified, which will be discussed in full in this paper. The modelling work is divided into two sub-parts, namely, a three-dimensional (3-D) modelling for the ink chamber and a two-dimensional (2-D) modelling for the nozzle-air domain. Simulations of the 3-D ink chamber were carried out firstly, thereby the transient mass flow rate of the ink outflow from the chamber could be obtained, which will be set as the inlet boundary condition of the 2-D nozzle-air simulations. To ensure accuracy and convergence of 2-D simulations, independence tests of the mesh grid and time step were performed, where the Fine level mesh density and 1e-8 s time step were identified as the optimal choice. And this combination was adopted in the transient simulations of the droplet ejection process. For the model validation purpose, an experimental test rig was developed, and comparisons between the simulations and experimental tests show a good agreement, verifying the accuracy of the developed model. In addition, to validate the feasibility of the developed model, the effect of the ink viscosity on the droplet ejection process was tested, and the results were consistent with those produced by published literature, confirming the feasibility of the CFD model developed in this paper.

Keywords: 3-D printing; PZT printhead; CFD; Two-phase flow.

NOMENCLATURE

D_3	electric field	β	fluid physical properties
E_3	electric stress	β_L	liquid physical properties
F	external force	β_G	gas physical properties
h	PZT movement displacement	ρ	density
S_1	strain	v	speed
T_1	stress	η	viscosity
U	driving voltage value	ρ_G	gas density
v	droplet speed	ρ_L	liquid density
ϵ_{33}^T	dielectric constant	η_G	gas viscosity
d_{31}	piezoelectric constant	η_L	liquid viscosity
S_{11}^E	elastic compliance coefficient		
f_L	liquid volume fraction		

1. INTRODUCTION

With the development of modern industry, three-dimensional printing (3DP) has become an indispensable emerging intelligent manufacturing technology in industrial productions (Wang *et al.*

2021), such as biomedical (Coakley 2014), aerospace (Wu 2013), mold manufacturing (Yang and Liu 2014) and ceramic manufacturing (Huang and Wu 2017), etc. In 3DP printing, droplet ejection technology is of great importance, and the printhead is a key component (Berman 2012; Liu *et al.* 2018). Among various types of printhead, the piezoelectric

(PZT) drop-on-demand (DOD) is the most used (Guo 2019), where the printing process can be controlled by the periodic excitation pulse signal exerted on PZT. Except for the PZT deformation, dynamics of the fluid flow inner the printhead is also critical. Performing accurate and efficient prediction on them is the premise of mechanism explorations and design optimizations, and it is also the objective of this paper.

With the development of computer technology, the computational fluid dynamics (CFD) method has been widely used in fluid flow related simulations, owing to its advantages of flow details available, low cost and high efficiency. However, due to the high nonlinearity and complexity of fluid flow, there is no CFD parameter can be suitable for all flow conditions. Therefore, to obtain a reasonable PZT printhead simulation model, it is necessary to conduct a special study on the CFD parameters for the 3DP printhead ejection structure.

With CFD method, many studies have been carried out by researchers in recent years, and different CFD parameters were adopted to simulate the dynamics of fluid flow. For example, Wu *et al.* (2005) established a 3-D numerical model to discuss the influence of critical parameters on the formation of droplet, where the volume of fluid (VOF) model was adopted for transient simulations. For the same purpose as Wu *et al.* (2005), Liou *et al.* (2009) studied the effects of nozzle size, ink properties and pressure waveform on the shape and velocity of the ejected droplet, where a 3-D axisymmetric CFD model comprising 175,000 mesh grids was developed to simulate the forming and ejecting process of a single droplet. The time step of the transient simulation was set to 10 ns, and SIMPLE algorithm was used for calculations. The results obtained from simulations were compared with those obtained from experimental tests, and a good agreement was observed, proving the effectiveness of the CFD parameters used in the simulation. In order to analyze the relationship between the driving waveform and the resonant pressure in the ink chamber, Liu *et al.* (2012) performed both numerical and experimental investigations on the droplet ejection process, and a good agreement was obtained between the simulations and the tests, however, the detailed CFD parameter settings were not mentioned. With the purpose of identify the influence of key parameters on the droplet ejections, a series of numerical simulations were conducted by Kim and Beak (2012), where the 2-D VOF model were adopted to calculate the process of droplet ejections. To reveal the mechanism of the droplet ejection, Zhou *et al.* (2013) established a 2-D axisymmetric CFD model for transient simulations, where the VOF model were adopted, however, the specific settings of the CFD parameters were not mentioned. To optimize the parameters of the trapezoidal wave of the driving signal, Wei *et al.* (2017) established a numerical model for transient simulations, where the laminar flow model was adopted to predict the effects of trapezoidal waves on the dynamics of the droplet ejection process. In order to discover the effects of different parameters on the droplet stable ejection

process, a 2-D axisymmetric CFD model was developed by Zhong *et al.* (2018), thereby transient simulation can be carried out. To verify the influence of ink viscosity value on droplet ejection, Lei *et al.* (2019) established a 2-D numerical to conduct transient simulations, where the laminar flow model was adopted.

The above research indicates that the CFD method has been widely used in PZT printhead related studies, such as mechanism exploration and performance optimization. However, to the best knowledge of the authors, few studies have specifically focused on the critical model settings for CFD simulations, such as timestep size of transient simulations, mesh grid density, eddy viscosity models and model dimensions, though both of these factors can have significant impact on the results and/or accuracy (Wu *et al.* 2005; Liou *et al.* 2009; Kim and Beak 2012). All of them will be discussed in full in this paper.

The remainder of this paper is organised as follows. First, the working principle of the printhead and the detailed information of the experimental test rig for the sand-printer PZT printhead are introduced (the results of experimental tests will be used as the criterion for model accuracy validation). Second, both 2-D and 3-D numerical model were developed, where the information of fluid domain identification, boundary condition settings, mesh grid independence tests, solver settings, optimal time-step size verifications, as well as model dimensional reduction methods were discussed in detail. Finally, the numerical simulation and experimental results are analysed and compared with the experimental tests, thereby the optimal CFD parameters for PZT printhead transient simulations can be identified.

In this study, the commercially available code ANSYS Fluent 19.0 was used for CFD simulations. In the CFD simulation, only the fluid dynamics is considered and not the behaviour of the PZT material.

2. DETAILS OF PZT PRINHEAD

A typical sand mould PZT printhead consists of multiple independent microdroplet nozzles with the same structure and principle, and each channel can be controlled independently. Figure 1 shows a simplified schematic of a PZT printhead droplet ejection unit. Each printhead unit consists of an ink chamber, a nozzle (in this study, the inner diameter of the print nozzle is 25 μm), a PZT membrane, piece of a metal film, and two electrodes bound to the PZT sheet.

The working process of the PZT printhead is as follows: when the excitation pulse is loaded on the PZT sheet, it expands and moves outward because of the converse piezoelectric effect, inflating the liquid chamber to draw the liquid from the liquid supply box. When the reverse excitation pulse is loaded on the PZT membrane, it will deform in reverse, and squeeze the liquid in the ink chamber to make it spray

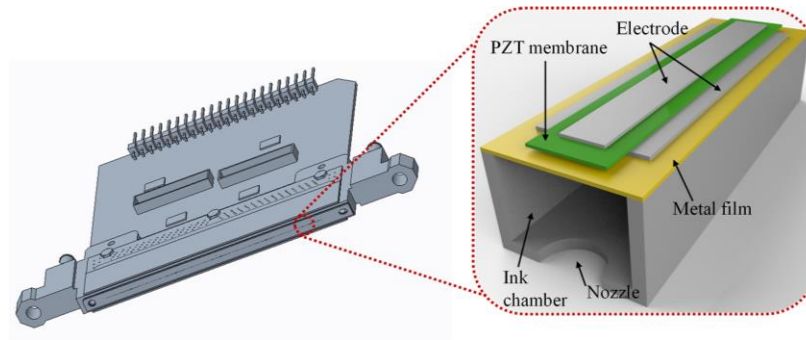


Fig. 1. Printhead droplet ejection unit.

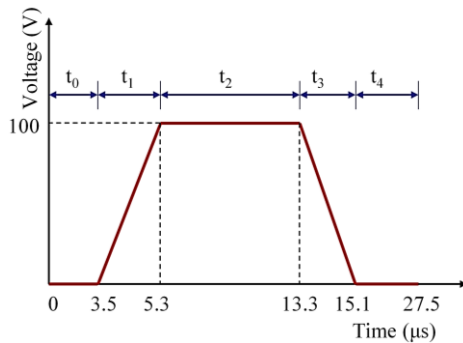


Fig. 2. Waveform used to drive the printhead.

out. After that, the PZT membrane will return to its initial position. The recovery action will generate negative pressure, which has the effect of pulling back the ink droplets that have not yet been discharged. The successive droplets that have been ejected will break up under the effect of surface tension and continue to move forward. By repeating the above steps, continuous printing can be achieved.

The deformation of PZT membrane is controlled by the excitation pulse exerted on it. Figure 2 shows a PZT excitation pulse with typical form, which consists of three sub-stages, namely, a rising sub-stage, a dwelling sub-stage, and a falling sub-stage. In this study, the excitation pulse shown in Fig. 2 was adopted to control the deformation of the PZT membrane.

The excitation pulse induced PZT membrane deformation will be used as the boundary condition of subsequent transient CFD simulation. To this end, the functional relationship between the excitation pulse and the membrane deformation should be analyzed first. According to the mathematical model proposed by [Wei *et al.* \(2003\)](#), the force displacement equation of the PZT actuator can be expressed as follow:

$$h = \alpha U - \beta F \quad (1)$$

where α and β are constants (their values are calculated using the method proposed by [Mu \(1983\)](#)) and U is the driving voltage, and the equation of PZT materials can be expressed as follows:

$$\begin{cases} S_1 = S_{11}^E T_1 + d_{31} E_3 \\ D_3 = d_{31} T_1 + \epsilon_{33}^T E_3 \end{cases} \quad (2)$$

where S_1 and T_1 are the strain and stress in the transverse direction, respectively; D_3 and E_3 are the longitudinal direction electric field and stress, respectively; ϵ_{33}^T is the dielectric constant when the external stress is zero or constant; d_{31} is the PZT constant and S_{11}^E is the elastic compliance coefficient when the electric field is equal to zero or constant. Only the longitudinal pressure value is considered in the PZT membrane displacement calculation. According to Eqs. (1)-(2) and the driving voltage, h_{\max} can be calculated as 14.1×10^{-6} mm.

However, in CFD simulations, the deformation of the PZT cannot be directly assigned, and the movement of the PZT membrane was expressed by the speed in every transient timestep. Thus, the speed trajectory of the PZT membrane should be calculated first. According to the research performed by [Pang \(2017\)](#), the speed trajectory of the PZT membrane movement can be approximated as a sinusoidal function curve, which can be calculated by given specific driving pulses. In this study, the key parameters of the driving pulse are the following: $t_1 = 1.8 \mu\text{s}$, $t_2 = 8 \mu\text{s}$ and $t_3 = 1.8 \mu\text{s}$. In addition, the speed trajectory of the PZT membrane movement shown by Fig. 3. was calculated, which will be assigned as a boundary condition in subsequent droplet ejection CFD simulations.

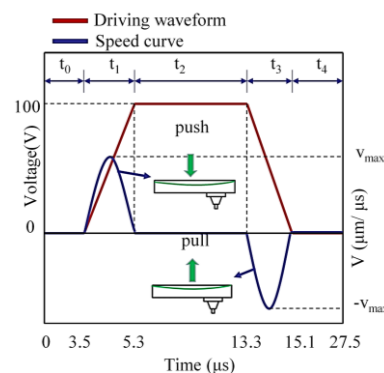


Fig. 3. Speed change curve.

3. EXPERIMENTAL TESTS

In this study, experimental tests were performed for CFD model accuracy validations. An experimental test rig was developed, as shown by Fig. 4, which is mainly composed of a droplet generation module and an observation module. The droplet generation module contains a control board, a pressure control system, ink boxes and a printhead. In the experimental tests, a Fujifilm sapphire QS256/80 AAA printhead with an array of 36 printing nozzles was used. The droplet-observation module contains a display system used to record the droplet ejection process, including a high-speed camera, and a flash with a high-intensity light-emitting diode. Furan resin was used as the ink liquid. Key parameters of the experimental tests are listed in Table 1.

Table 1. Experimental parameters.

Observation module		Droplet generation	
Pixel	1032 × 778	Printhead type	QS256/80 AAA
Voltage amplitude	5 V (TTL)	Voltage amplitude	100 V
Frequency	80 kHz	Frequency	8 kHz
Focal length	6:1	Ink viscosity	12.5 cp (25°C)
Pulse width	0.25 μs	Ink type	Furan resin
Supply Voltage	220 V		

In the experiments, the distance between the printhead and the deposition substrate was set to 2 mm to enable the ejected droplets to develop fully. Each inkjet channel could be individually controlled, and the observation system is aligned with one channel to better monitor the shape and position changes of droplet. The firing signal from the printhead can be transmitted to the cameras, enabling them to take pictures at the same operating frequency.

The experimental process is as follows. First, set the pulse voltage of the printhead and ejection frequency to 100 V and 8 Hz, respectively, (as shown by Table 1). Second, set the excitation pulse width values, t_1 , t_2 , t_3 , t_4 and t_5 (according to values shown in Fig. 2). Third, start the camera and printhead to capture and record the transient shape and position of the ejected droplets. By setting different driving pulses, the droplet pictures at different times can be recorded as the camera is refreshed. To ensure the accuracy of the experimental tests, several repeated tests with the same excitation pulse were conducted, and pictures obtained from different tests were compared. The results showed that the droplets can be ejected continuously, and the shapes and transient positions of the ejected droplets are almost identical, confirming the reproducibility of the developed experimental test rig and the feasibility of the test procedure.

4. NUMERICAL ANALYSIS

4.1 Basic Theory

The principle of CFD simulation is to solve the governing equations with given boundary conditions in designated fluid domains (Zong *et al.* 2020). Different from single-phase simulations, numerical analysis of the PZT printhead requires exploring the interactions between two different phases, namely, the air and the liquid ink. To overcome this, the VOF model was utilised (Mondal and Chatterjee 2016). In this model, the free surface flow of the droplet was tracked using the volume fraction equation (Liu 2010), which is provided as follows:

$$\frac{\partial f_L}{\partial t} + v \cdot \nabla f_L = 0 \quad (3)$$

where f_L is the liquid volume fraction of each control volume and v is the droplet speed. For the two-phase flow model, the physical properties of each control volume are calculated based on the value of f_L . The f_L value is specified as follows: when 0 or 1 is assigned to f_L , the calculation grid is

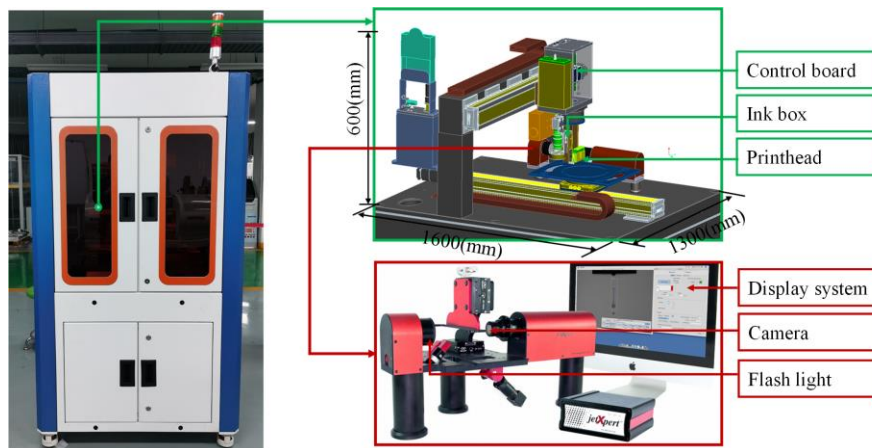


Fig. 4. Experimental platform.

filled with air or liquid, respectively. If $0 < f_L < 1$, this implies that the air and liquid phases intersect in the calculation grid. Therefore, the physical properties in the cell are expressed as follows:

$$\beta = f_L \cdot \beta_L + (1 - f_L)\beta_G \quad (4)$$

where β is the physical property of the fluid in the cell, β_L is the physical property of the liquid phase and β_G is the physical property of the gas phase.

On the basis of this description of the fluid properties, when the PZT printhead expels droplets, the continuity and Navier–Stokes equations are established as follows:

$$\frac{\partial \rho}{\partial t} + \nabla \cdot (\rho v) = 0 \quad (5)$$

$$\frac{\partial}{\partial t} (\rho v) + \nabla \cdot (\rho v v) = -\nabla p + \nabla \cdot [\eta (\nabla v + \nabla v^T)] + \rho g + F \quad (6)$$

where ρ is the density, v is the speed, p is the pressure, η is the viscosity and F is the volume force. The density value ρ can be solved using Eq. (2), and the viscosity value η is calculated from the following formula:

$$\eta = \frac{f_L \rho_L \eta_L + f_G \rho_G \eta_G}{f_L \rho_L + f_G \rho_G} \quad (7)$$

where ρ_G and ρ_L represent the density of gas and

liquid, respectively, η_G and η_L represent the viscosity of gas and liquid, respectively.

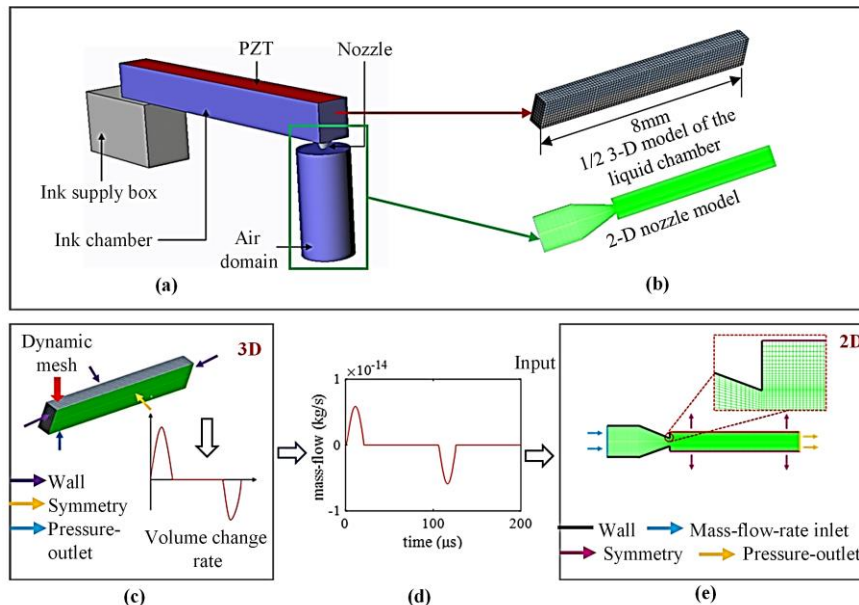
4.2 CFD Model Development

In the CFD simulation model used in this study, the ink chamber was always full of ink during the calculation. Furthermore, a new simulation method was built to improve the simulation efficiency. First, the 3-D model was split into two parts (shown in Fig. 5). The first part is the ink chamber with an upper sidewall consisting of a PZT. The second part is the nozzle, connecting to the air domain.

As shown in Fig. 5(b), in simulation, 3-D and 2-D models were developed for the ink chamber and nozzle, respectively. For the 3-D ink chamber model, the dynamic mesh technology was adopted to simulate the movement trajectory of PZT membrane, thereby the curve of volume changes could be recorded simultaneously. On the basis of the volume change curve, the transient mass flow rate of the fluid outflow from the ink chamber was calculated, and it will be set as the inlet boundary conditions of the 2-D nozzle model.

4.2.1 The 3-D model of the ink chamber

In this study, the main function of 3-D simulation was to obtain the transient mass flow rate outflow from the ink chamber, which will be used as the inlet boundary condition of 2-D nozzle model. To perform 3-D simulations, mesh grid for liquid ink chamber was developed, and a total of 50,000 cells were generated. For the transient simulations, a very small timestep, namely, 100ns was adopted to ensure that all features of the volume change curve were captured.



(a) The fluid domain of the ink chamber and printhead, (b) 3-D/2-D models for the ink chamber/nozzle, (c) the boundary conditions of 3-D ink chamber model, (d) the mass flow rate obtained for 3-D ink chamber simulations (e) the boundary conditions of 2-D nozzle models.

Fig. 5. Single nozzle model decomposition method.

To simulate the deformation of the PZT membrane, the wall representing the PZT membrane was defined as a deforming wall, and the dynamic mesh technology and the layering method were used to change the velocities and positions of the mesh grid representing the PZT membrane. The other sidewalls of the ink chamber were defined as stationary wall with no slip shear condition.

To reproduce the deformation of the PZT membrane, the user-defined functions (UDFs) method was applied to control the movement of grid nodes inner the PZT membrane deforming wall. With the deformation of the PZT, the cross section of ink chamber will also be changed, as shown by Fig. 6, representing the volume change of the ink chamber, and it is corresponding the mass flow inlet of the nozzle part of printhead.

Figure 6 shows a schematic of the cross section when the PZT membrane is compressed to its lowest point, where h_{max} is the maximum compression displacement and W is the width of the PZT membrane. The velocity curve of the PZT membrane and its maximum stroke (h_{max}) are expressed as follows:

$$f(t) = A \sin \omega \bullet t \tag{8}$$

$$h_{max} = \int_0^T A \sin \omega t dt \tag{9}$$

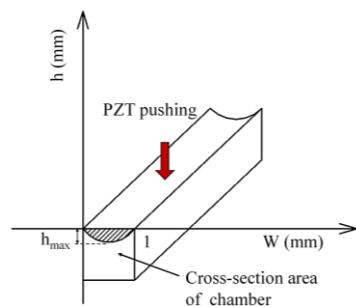


Fig. 6. Movement of the PZT membrane.

On this basis, the velocity curve of the PZT membrane movement can be expressed as follows:

$$f(t) = \begin{cases} A \sin \omega t, & 0 \leq t < 1.8 \times 10^{-6} \\ 0, & 1.8 \times 10^{-6} \leq t < 1.04 \times 10^{-5} \\ A \sin \omega(t - t'), & 1.04 \times 10^{-5} \leq t < 1.22 \times 10^{-5} \\ 0, & t > 1.22 \times 10^{-5} \end{cases} \tag{10}$$

where $A = 0.015$, $\omega = 2.1 \times 10^6$ and $t' = 8.5 \times 10^{-6}$.

For the transient simulations, Eq. (10) was programmed by using DEFINE_GRID_MOTION macro of UDF method and compiled into the commercially available code Fluent 19.0. Meanwhile, the area change of the chamber cross-sectional area was recorded by using the DEFINE_ADJUST macro. And the mass flow rate outflow the ink chamber was calculated by using the DEFINE_EXECUTE_AT_END macro.

Before the simulation, the liquid volume fraction was initialised to 1 through the region adapter and patch

functions. After one ejection cycle, the ink in the chamber was automatically replenished by gravity. Thus, in the simulation of the 3-D chamber model, the chamber was full of ink by default every time it was ejected.

4.2.2 The 2-D model of the nozzle

For the CFD simulations, the eddy viscosity model has great influence on the accuracy and convergence of the calculation. Therefore, to identify the optimal eddy viscosity model, the Reynolds value of the flow was calculated using empirical Eq. (11):

$$Re = \frac{\rho v d}{\mu} \tag{11}$$

where ρ is the density of the liquid, v is the speed of the droplet outlet, d is the diameter of the nozzle and μ is the viscosity of the liquid.

The result shows that the Reynolds number of the flow was found to be 15, which means that the fluid flow was laminar. Therefore, a laminar model was used for the initial CFD simulations. However, the comparison between the CFD simulations and experimental tests show that there are obvious differences in the droplet shapes and velocities after droplet ejection, as shown in Fig. 7. To explore the

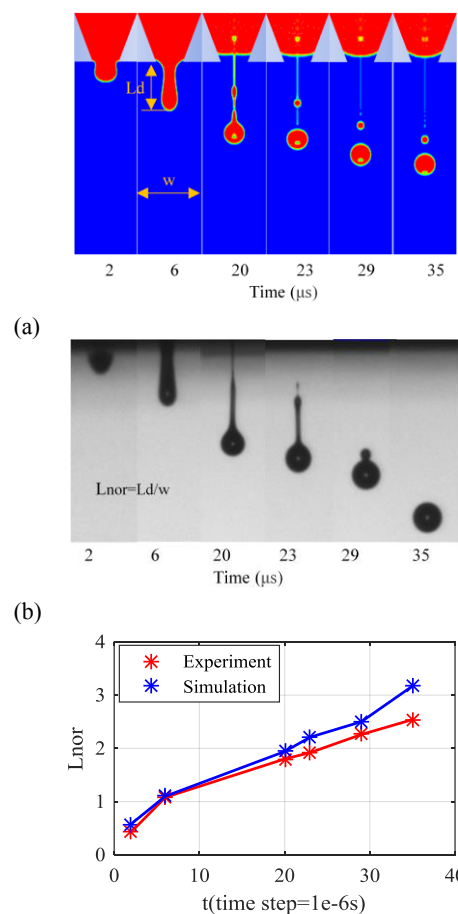


Fig. 7. Comparison of the droplet ejection (a) calculated by the laminar model, (b) obtained by experimental tests, (c) comparison of the transient droplet positions.

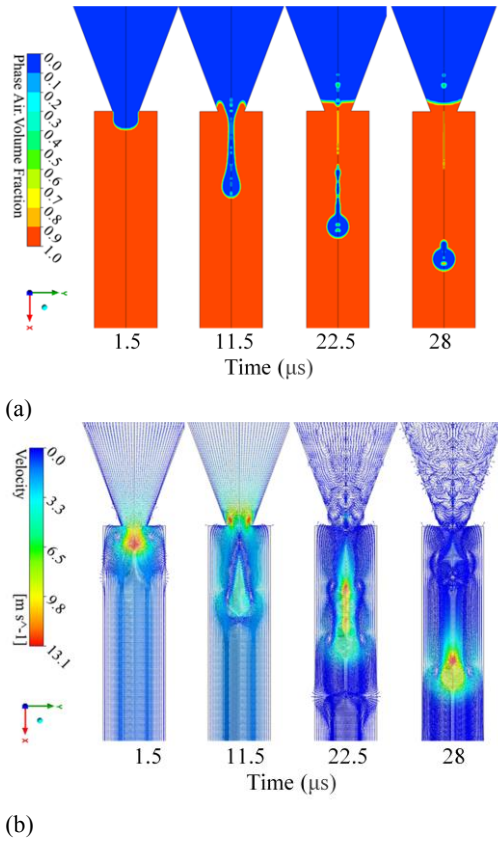


Fig. 8. Flow contours and vectors of the fluid.

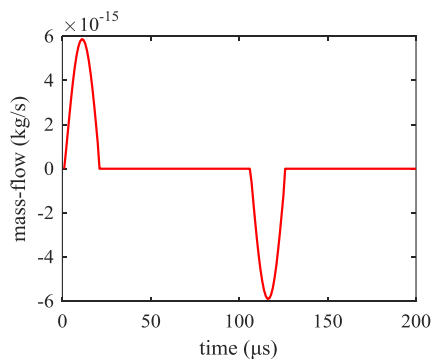


Fig. 9. Mass flow rate input curve.

causes, the phase contours and vectors of the ejection process were analyzed, as shown in Fig. 8, which indicates that the flow in the liquid and air regions are in laminar state initially, but will turn to turbulent when the droplet was ejected out of the nozzle, obvious vortexes were shown, meaning that the laminar model is not suitable any more.

Therefore, to capture the flow characteristics as accurately as possible, the Standard k-epsilon turbulence model used for CFD simulations in this paper, owing to its advantages of easy convergence and high computational efficiency.

For the transient CFD calculations, both of mesh grid density and timestep size have great influence on the results. Therefore, to ensure the accuracy and convergence of the PZT printhead simulations, independence tests for the grid density and time

Table 2. Parameter settings for simulations.

Parameter	Values
Fluid	Newtonian fluid
Analytical model	Turbulence model
Solution method	PISO scheme
	Second-order
Viscosity	12.5 cp (20°C)
Density	1500 kg/m ³
Surface tension	0.065 N/m (20°C)
Maximum iteration steps	200

Table 3. Results of the grid independence tests.

Time step size /s	Normalised Distance		
	Coarse	Fine	Very Fine
1e ⁻⁷	1.683	1.867	1.867
1e ⁻⁸	1.717	1.900	1.900
1e ⁻⁹	1.833	1.917	1.900

interval needed to be performed first. In independence tests, three levels of mesh grid densities (Coarse (16,634), Fine (20,634) and Very Fine (58,334)) and 3 level of timestep sizes (1e⁻⁷, 1e⁻⁸ and 1e⁻⁹ s) were adopted, the other parameters and solver settings are shown in Table 2.

The inlet of the 2-D model was defined as the mass flow inlet, and its specific value is expressed by Eq. (12), whose curve is shown in Fig. 9.

$$\dot{m} = \begin{cases} a \cdot t^5 + b \cdot t^4 + c \cdot t^3 + d \cdot t^2 + e \cdot t, & t \in A \\ 0, & t \in B \\ a \cdot (t - g)^5 + b \cdot (t - g)^4 + c \cdot (t - g)^3 + d \cdot (t - g)^2 + e \cdot (t - g), & t \in C \\ 0, & t \in D \end{cases} \quad (12)$$

Where A = (0, 1.8 × 10⁻⁶), B = (1.8 × 10⁻⁶, 1.04 × 10⁻⁵], C = (1.04 × 10⁻⁵, 1.22 × 10⁻⁵], D = (1.22 × 10⁻⁵, 0), a = 3.193 × 10¹⁴, b = 2.885 × 10⁹, c = -6.893 × 10³, d = -2.808 × 10⁻⁴, e = 8.362 × 10⁻⁹ and g = 8.5 × 10⁻⁶.

The results of mesh grid and timestep independence tests are shown in Table 3 and Fig. 10. A total of Nine different combinations of mesh and timesteps were simulated, and shapes and transient positions (at t = 20 μs) of the ejected droplets were compared. The position of the droplet was expressed by length index of L_{nor} = d/w, where d is the length of the droplet and w is the width of the air domain. As shown in Table 3 and Fig. 10, both mesh grid density and timestep size have great influence on printhead CFD simulations. For mesh grid, when the density changed from Coarse to Fine, the shapes and locations of the ejected droplets shown by the phase contours were very different, however, continue. However, as the grid density increased from Fine to Very Fine, there was no obvious change in the shapes and locations of the droplets, which means that the simulation converges for grid densities greater than

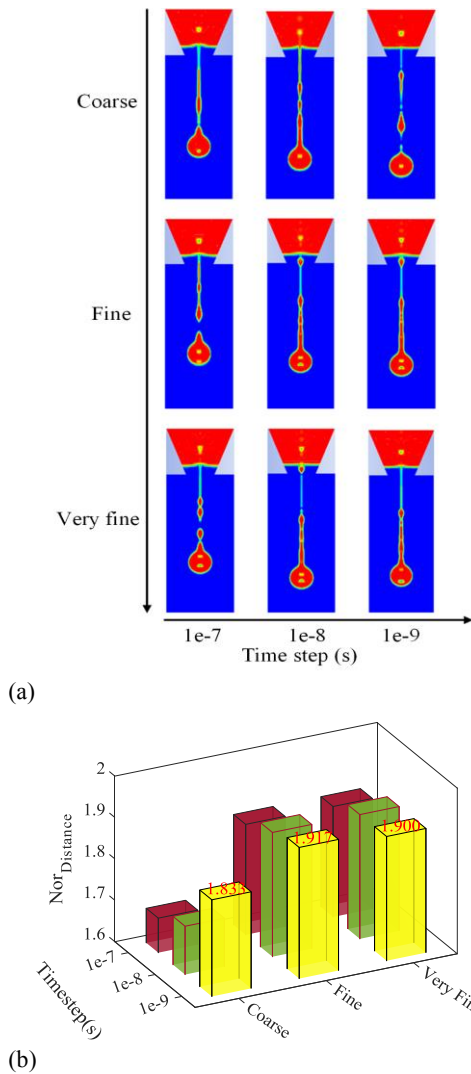


Fig. 10. Droplet ejection results: (a) the phase contours at $t = 20 \mu\text{s}$ and (b) the values of L_d at different time steps and mesh densities.

the Fine level. For the timesteps, a similar result is also obtained, namely, the simulation results changed greatly when the timestep size change from $1e^{-7}$ to $1e^{-8}$, and when it was further reduced, the simulations produced similar results for the shapes and positions of the droplets. Summarize the test results of mesh grid and timestep size, it can be concluded that when the mesh grid density is higher than the Fine level, while the size of transient timestep is smaller than $1e^{-8}$ s, the results of the CFD simulations were independent of the mesh and timestep. In this study, for efficiency and computing resource saving consideration, the Fine level mesh grid combined with the $1e^{-8}$ s timestep size were adopted for the transient simulations of the printhead droplet ejections.

5. RESULTS AND DISCUSSION

5.1 Model Accuracy Validation

In this part, the accuracy of the developed CFD model was validated by experimental tests. The

droplet ejection process (including droplet shapes, transient positions, satellite droplet formations and droplet neck breakage), obtained from the transient CFD simulations were compared with those obtained from experimental tests.

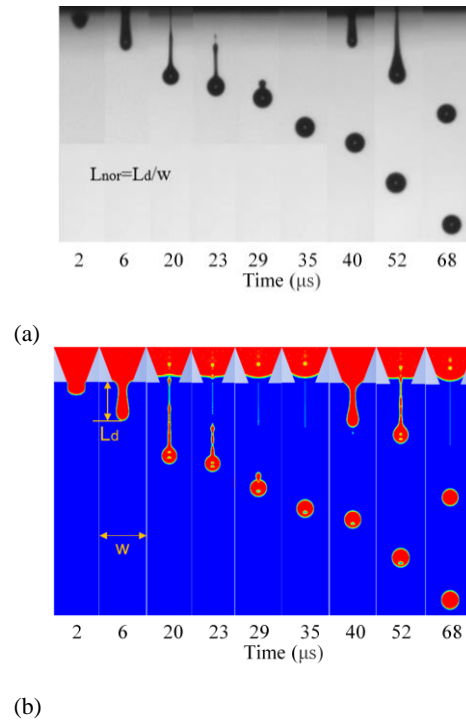


Fig. 11. Comparison of (a) an experimental test and (b) a CFD simulation.

For the droplet ejection process, as shown by the results obtained from experimental tests (Fig. 11(a)), initially, a meniscus-like shape droplet was formed and ejected from the nozzle ($0-1.85 \mu\text{s}$), after that, the droplet continued to move until its neck broke ($1.85-21 \mu\text{s}$), and it formed a spherical droplet under the effect of surface tension, and continued to move forward ($21-35 \mu\text{s}$).

Figure 11(b) shows the results of the droplet ejection process obtained from CFD simulations. For comparison purpose, a length index L_{nor} was defined to quantify the transient position of the ejected droplet (the distance from the nozzle outlet to the front edge of the droplet). The result of comparison between the experimental tests and the CFD simulations is shown in Fig. 12, indicating a very close agreement between the transient positions of the ejected droplets at different time points are very close, meaning that the CFD model developed in this paper has a good ability in droplet position and velocity predictions. In addition to the droplet transient position, the shape of the ejected droplets was also compared, as shown in Fig. 11, also showing good agreement and confirming the ability of the developed CFD model in droplet shape predictions.

In addition to the 2-D model, the influence of mesh grid dimensions on the transient CFD simulation of

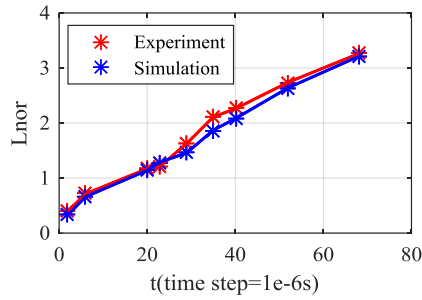


Fig. 12. Comparison of the droplet length between the 2-D simulations and the experimental tests.

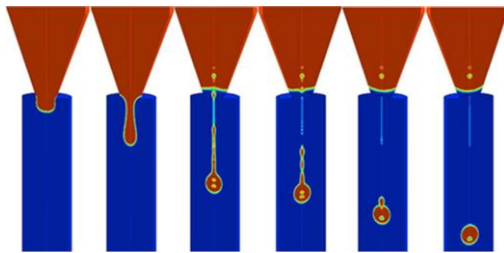


Fig. 13. Results of the 3D simulations.

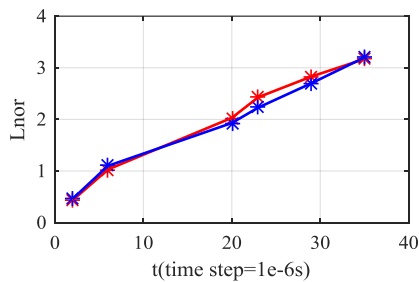


Fig. 14. Comparison of the droplet length between the reduced-order model and 3-D printhead model.

the droplet ejection process was also identified. A 3-D mesh model for the nozzle–air domain part was developed, and the results obtained from 2-D and 3-D simulations were compared, as shown in Figs. 13–14, indicating that the shape and transient positions of the ejected droplets are very close. This means that the dimension of the mesh model does not have an obvious effect on the simulations of the droplet ejection process, namely, the 2-D model adopted in this paper is reasonable.

Since the ejection process of the printhead is continuous, the previous droplet ejection may affect the subsequent process. To identify this effect, a two-cycle simulation of the droplets were also performed, as shown in Fig. 11(b). By comparison with the experimental tests shown in Fig. 11(a), the shape and velocity of the first and second droplets were almost identical, which means that the first ejection had no obvious effect on the second droplet ejection.

5.2 Feasibility Validations

To verify the effectiveness of the developed model, additional simulations were carried out to explore the effect of ink properties on the process of droplet ejections, where the ink viscosity was changed from 12.0 to 15.0 cp, while all other parameters of the nozzle simulation model remain unchanged. The comparison between the results obtained from different ink viscosities is shown in Fig. 15, indicating that increasing viscosity value will reduce the velocity of droplets and lead to fewer satellite droplets. This result is consistent with that produced by *Zhong et al.* (2018), which confirms the feasibility of the CFD model and simulation method adopted in this paper.

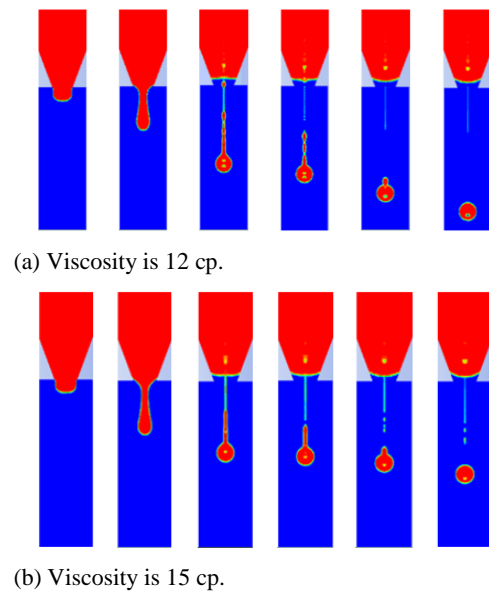


Fig. 15. Effect of ink viscosity on droplet ejection.

6. CONCLUSIONS

This paper performed a numerical analysis on the flow dynamics of the Piezoelectric Inkjet Printhead, of particular concern is the method of transient CFD model development and the accuracy validation of the developed model. For the method of CFD modelling, 3-D and 2-D numerical model were developed for the ink chamber and the nozzle–air parts, respectively. Independence tests of mesh grid and timestep size of transient simulations were performed, and UDF method was adopted to transfer the result of 3-D ink chamber simulation to 2-D nozzle–air part simulation (namely, the mass flow rate of ink outflow the ink chamber, which was used as the inlet boundary condition of the 2-D simulation). To validate the accuracy of the model, the simulation results were compared with those obtained from experimental tests, both the abilities in droplet shape and transient positions predictions were tested. The conclusions of this study can be summarized as follows.

a) For the CFD parameters, the effects of eddy viscosity model, the mesh grid, and the transient timestep size on the prediction of droplet ejection were analysed. The results showed that the Standard k-epsilon turbulence model, the Fine level mesh grid and $1e^{-8}$ s timestep size are the optimal CFD setting combination of simulations of droplet ejection process in this paper.

b) For the model dimensions, both 2-D and 3-D model of the nozzle-air part were developed, and the results were compared, showing that the shape and transient positions of the ejected droplets were very similar, which means that the dimensions of the mesh model do not have an obvious effect on the simulations of the droplet ejection process, namely, the 2-D model adopted in this paper is reasonable.

c) To validate the accuracy of the model, results obtained from CFD simulations and experimental tests were compared, which indicates that the shapes and transient positions of the ejected droplets were in close agreement, confirming the accuracy of CFD model and simulation procedure adopted in this paper.

d) To test the feasibility of the model, additional simulations were performed using ink of different viscosities while keeping all other parameters identical. The results showed that, compared with 12 cp ink, the droplet velocity of 15cp ink were reduced, which is also consistent with that produced by [Zhong et al. \(2018\)](#), confirming the feasibility of the CFD model developed in this paper.

ACKNOWLEDGEMENTS

The research described in this paper was financially supported by the National Natural Science Foundation of Ningxia (2021AAC03196) and the Important Science and Technology Specific Projects of Anhui Province (S202003a05020087).

REFERENCES

- Berman, B. (2012). 3-D Printing: The new industrial revolution. *Business Horizons* 55(2), 155-162.
- Coakley, M. F., D. E. Hurt, N. Weber, E. C. Fincher, D. T. Chen, A. Yun, M. Gizaw, J. Swan, S. Y. Terry and Y. Huyen (2014). The NIH 3D print exchange: a public resource for bioscientific and biomedical 3D prints. *3D Print Addit Manuf* 1(3), 137-140.
- Guo, L. (2019, July). *The Drop Generation Mechanism and Regulation of Drop-on-demand Electrohydrodynamic Jet Printing*, Ph. D. thesis, Huazhong University of Science & Technology, Wuhan, China.
- Huang, M. J. and H. D. Wu (2017). Research progress of ceramic additive manufacturing (3D printing) technology. *Advanced Ceramics* 38(04), 248-266.
- Kim, E. and J. Beak (2012). Numerical study on the effects of non-dimensional parameters on drop-on-demand droplet formation dynamics and printability range in the up-scaled model. *Physics of Fluids* 24(8).
- Lei, X. X., Y. Ye and N. Ling (2019). Effect of viscosity on droplet volume during inkjet printing. *Chinese journal of luminescence* 40(08), 1040-1048.
- Liou, T. M., C. Y. Chan and K. C. Shih (2009, May). Effects of actuating waveform, ink property, and nozzle size on piezoelectrically driven inkjet droplets. *Microfluidics and Nanofluidics* 8(5), 575-586.
- Liu, H., Y. Gao, S. H. Ding, F. Peng and D. X. Zhu (2018). Research on the effect of the waveform on the droplet injection behavior of a piezoelectric printhead and the forming accuracy of casting sand molds. *The International Journal of Advanced Manufacturing Technology* 100(1-4), 251-261.
- Liu, Y. F., Y. F. Pai, M. H. Tsai and W. S. Hwang (2012). Investigation of driving waveform and resonance pressure in piezoelectric inkjet printing. *Applied Physics A* 109(2), 323-329.
- Mondal, B. and D. Chatterjee (2016). Numerical investigation of the water droplet transport in a PEM fuel cell with serpentine flow channel, *Journal of Applied Fluid Mechanics* 1057-1071.
- Pang, J. W. (2017, Sep.). *Modeling and Analysis of a Novel Piezoelectric Driven Micro-positioning Stage*. M.S. thesis, Shandong University, Shandong, China.
- Wang, M., Y. Wang, J. Liu, Y. Xu and X. Liu (2021). Standards system construction in key areas of manufacturing industry. *Strategic Study of CAE* 23(03), 16-24.
- Wei, D. Z., R. J. Zhang and R. D. Wu (2003, July). Mathematical model of piezoelectric actuated micro-droplet jetting process. *China Mechanical Engineering*, 611-614.
- Wei, H. F., X. L. Xiao, Z. F. Yin, M. C. Yi and H. L. Zou (2017). A waveform design method for high DPI piezoelectric inkjet print-head based on numerical simulation. *Microsystem Technologies* 23(12), 5365-5373.
- Wu, H. (2013). The status quo and development ideas of 3D printing industry. *Technology Wind* (24), 277.
- Wu, H. C., H. J. Lin, and W. S. Hwang (2005). A numerical study of the effect of operating parameters on drop formation in a squeeze mode inkjet device. *Modelling and Simulation in Materials Science and Engineering* 13(1), 17-34.
- Yang, Y. Q. and W. H. Liu (2014). Application of ink-jet sand 3D printing technology in engine cylinder block trial-production. *China Academic Journal Electronic Publishing House*.

Zhong, Y.H., H. S. Fang, Q. L. Ma and X. R. Dong (2018). Analysis of droplet stability after ejection from an inkjet nozzle. *Journal of Fluid Mechanics* 8(45), 378-391.

Zhou, S. G. (2013, July). *Simulation and Experimental Study on Piezoelectric Diaphragm-driven Microdroplet Jetting Technology*. M.S. thesis, Shanghai Jiao Tong

University, Shanghai, China.

Zong, C.Y., F.J. Zheng, D.J. Chen, D. William and X.G. Song (2020). Computational Fluid Dynamics Analysis of the Flow Force Exerted on the Disk of a Direct-Operated Pressure Safety Valve in Energy System. *Journal of pressure vessel technology*142:011702